American Mineralogist, Volume 81, pages 1476–1493, 1996

Observations on the geometry of etched fission tracks in apatite: Implications for models of track revelation

RAYMOND JONCKHEERE* AND PETER VAN DEN HAUTE

Geologisch Instituut, University of Gent, Krijgslaan 281, B9000 Gent, Belgium

ABSTRACT

This paper reports observations of etched internal {0001}, {10$\bar{1}$0}, {11$\bar{2}$0}, {10$\bar{1}$1}, and {11$\bar{2}$1} surfaces of Durango apatite. Three types of surfaces are distinguished: P type, S type, and T type. After initially acquiring a certain roughness, P-type surfaces grow smoother with etching time. S-type surfaces remain smooth for long etching times. T-type surfaces develop a progressively coarser texture. Polishing scratches are flat bottomed in P-type, sharp in S-type, and indistinct in T-type surfaces. Fission tracks are funnel shaped in P-type surfaces but simple channels in S- and T-type surfaces. Several lattice defects other than fission tracks are revealed in P-type surfaces but not in S- and T-type surfaces. S-type surfaces can retain the imprints of fission tracks after they have been etched out. The etching velocity perpendicular to the surface increases in the order of P, S, T. Track density is approximately the same in all surfaces near the limit of track revelation but diverges with prolonged etching. It decreases in P-type surfaces, remains fairly constant in T-type surfaces, and increases in S-type surfaces. These trends are partly explained by the interplay between the track geometries and the track-determination criteria. The classic v_b-v_t model fails to explain these track geometries or their dependence on surface orientation. An alternative model is proposed, based on the theories of crystal growth and dissolution. This model implies that the efficiency of fission-track counts cannot be calculated on the basis of etching velocities. It further predicts that confined track lengths do not increase indefinitely with etching time, and that the lengths of surface tracks decrease.

INTRODUCTION

Fission tracks in apatite are revealed by etching before they are counted and measured. As a result, reported track densities and track lengths refer to etched fission tracks. The annealing equations, describing track length or track-density reduction as a function of temperature and time, have equally been established on the basis of measurements of etched tracks (e.g., Green et al. 1985; Laslett et al. 1987; Crowley et al. 1991). The phenomenon of annealing is itself almost exclusively understood at the level of etched tracks, i.e., as a reduction of etchable track length, which does not necessarily correspond to a shortening of the distorted region that constitutes the latent fission track (Paul and Fitzgerald 1992; Paul 1993). The mechanism of track revelation in apatite, and in anisotropic detectors in general, has however received little attention in comparison with track revelation in isotropic detectors and is not yet fully understood.

Models of track revelation in isotropic detectors are based on two velocities: the track-etching velocity, v_t, and the bulk-etching velocity, v_b (Fleischer et al. 1975; Wagner and Van den haute 1992). The former represents the velocity at which the etchant penetrates the damaged material along the track. The latter represents the velocity at which the exposed, undamaged material is removed in different directions. Track revelation in anisotropic detectors is sometimes represented in a similar fashion. Anisotropy is considered either by accepting that the magnitude of v_b varies with orientation (e.g., as the radius of an ellipsoid; Thiel and Külzer 1977) or by assuming that v_b acts parallel to certain lattice planes (Wagner 1969; Somogyi 1980).

Earlier observations have brought to light the influence of the crystallographic orientation of the etched surface on the geometry of etched fission tracks in different minerals (Fleischer and Price 1964; Maurette et al. 1964; Wagner 1969; Gleadow 1978). It is well known that etched tracks are often knife-blade shaped in the prism faces of apatite and funnel shaped in the basal face. They are also bounded by a set of approximately flat planes, which clearly distinguishes them from the cone-shaped tracks in isotropic detectors. Even a modified v_b-v_t model cannot account for these complex track geometries or for their dependence on surface orientation. A new model is therefore necessary to describe track revelation in anisotropic detectors.

When Price and Walker (1962) published their etching experiments, the growth and dissolution of crystals and the revelation of defects in semiconductor surfaces were

* Present address: Max-Planck Institut für Kernphysik, Saupfercheckweg, 1, D-69117 Heidelberg, Germany.

0003–004X/96/1112–1476$05.00

already well-established fields of research. The issuing theories provide valuable insights into the revelation of fission tracks in minerals but have remained largely unnoticed by fission-track geochronologists. We attempted to apply concepts borrowed from the theories of crystal growth and dissolution to interpret observations of the geometry and density of etched fission tracks in different crystallographic planes of apatite.

Experiments

The experiments involved 14 sections, measuring 1 mm thick, cut from a single crystal of Durango apatite. Durango apatite is an age standard for fission-track dating (Hurford 1990) and is described in detail by Paulick and Newesely (1968) and Young et al. (1969). The sections were cut along different orientations (to within 5°), using a Struers Acutom apparatus equipped with a 0.1 mm diamond blade. Each section was mounted separately in epoxy resin (Araldit, Ciba Geigy) and ground with 600, 800, and 1000 mesh corundum powders. The flat internal surfaces thus obtained were subsequently polished on a Struers DP-U4 polishing apparatus using, in succession, 6, 3, and 1 μm diamond sprays (Struers DP-spray).

The first objective was to study the geometry and measure the density of etched fission tracks in apatite in relation to the crystallographic orientation of the etched surface. This was performed on a set of five sections (set A), cut parallel to the {0001}, {10$\bar{1}$0}, {11$\bar{2}$0}, {10$\bar{1}$1}, and {11$\bar{2}$1} planes, respectively (Fig. 1). These sections were neither annealed nor irradiated and therefore contained only spontaneous tracks. Set A was etched in a 2.5% nitric acid solution at 25 °C. Each sample was etched in five consecutive 60 s steps. After each step, it was ultrasonically cleaned, washed in pure ethanol, and oven dried at 60 °C. One-fifth of the apatite surface was then covered with adhesive tape, which shielded it from further corrosion during the next etching step. Thus, after five steps, each sample was divided into five adjoining regions in which the tracks were etched for 60, 120, 180, 240, and 300 s, respectively.

The second objective was to study the evolution of different surfaces with prolonged etching and to measure their respective etching velocities. A second set of five sections (set B) with the same orientations as set A was heated for 10 h at 450 °C to anneal the fossil tracks. Set B was not irradiated either; therefore, these sections contained no fission tracks. They were etched in a single 1800 s step in a 2.5% nitric acid solution at 25 °C. Part of the apatite surfaces was also covered with adhesive tape prior to etching.

A preliminary study of the influence of etchant concentration on track geometry was performed on two additional sets, C and D, consisting of two slices each: one parallel to {0001} and one parallel to {11$\bar{2}$0}. Sets C and D were neither annealed nor irradiated and therefore contained only spontaneous tracks. Set C was etched for 60 s in 25% HNO_3 at 25 °C. Set D was etched for 1800 s in 0.25% HNO_3 at 25 °C.

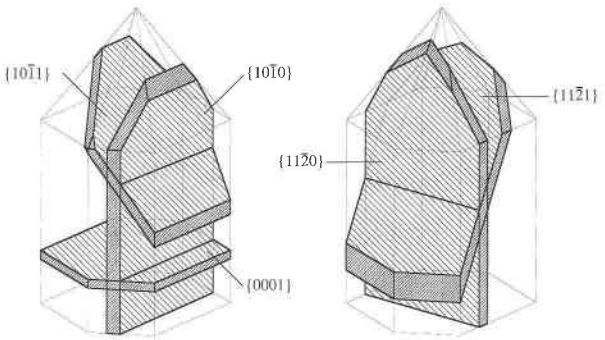

Figure 1. Diagram showing the relative orientations of the studied {0001}, {10$\bar{1}$0}, {11$\bar{2}$0}, {10$\bar{1}$1}, and {11$\bar{2}$1} sections of Durango apatite. The crystal, shown for reference, is bounded by {10$\bar{1}$0} prismatic faces and {10$\bar{1}$1} pyramidal faces, which are usually prominent in crystals of Durango apatite.

Plastic replicas were made of all 14 etched sections. A drop of acetone was applied to the surface and immediately covered with 1 cm^2 of acetate foil (Dr. Stock). The foil was removed after 120 s and the procedure repeated a second time. The first replica removed the last remaining impurities trapped in the tracks. The second provided a nearly perfect plastic cast of the surface topography, including the track openings and track channels. The track orientations were somewhat disturbed, however, on removing the replica from the apatite surface.

Track geometries were studied under the optical microscope with the use of transmitted and incident illumination and under the scanning electron microscope. Surface topography and track openings were studied on the etched apatite surfaces. Details of the track geometries were studied on scanning images of the replicas. For practical reasons different electron microscopes had to be used for observations of set A (Jeol JSM 6400), set B (Philips SEM 505), and the replicas (Jeol U3). Of sets C and D, only the replicas were studied under the electron microscope.

Track-density measurements were performed on set A with an Olympus-BH2 microscope under transmitted light, using 100× dry objectives and 10× eye pieces. The overall magnification of the microscope image included a drawing tube factor of 1.25×. Its actual value, calibrated against a stage graticule, was 1274×. The thickness of the apatite layer removed by etching was measured on set B by focusing first on a point on the unetched part of the surface and then on a nearby point on the etched part. The vertical distance between both points was read from the micrometer scale on the fine-focus knob of the microscope. Its accuracy was checked against the manufacturer-specified thickness of a microscope slide and proved good. The mean of 20 measurements was taken as the final estimate of the thickness removed.

Observations

Track geometry and surface orientation

Surface types. The five sections in sets A and B fall into three groups, as listed in Table 1. The P-type sec-

TABLE 1. Measured radial shift velocities (v_r) of five crystallographic planes of apatite

Section	Type	h (μm)	t_e (min)	v_r (μm/min)
{0001}	P	2.3(2)	30	0.08(1)
{11$\bar{2}$1}	P	8.0(2)	30	0.27(1)
{11$\bar{2}$0}	S	11.2(2)	30	0.37(1)
{10$\bar{1}$0}	T	19.2(3)	30	0.64(1)
{10$\bar{1}$1}	T	18.3(1)	30	0.61(1)

Note: Data for set B: 2.5% HNO_3, 1800 s, 25 °C; $v_r = h/t_e$, where h = height of the threshold between the etched and unetched parts of the apatite surface, and t_e = etching time. Errors are quoted at the 1σ confidence level.

tions, {0001} and {11$\bar{2}$1}, are characterized by broad, flat-bottomed polishing scratches. Fission tracks show a typical funnel shape, and several crystal defects other than fission tracks are also revealed. The S-type section, {11$\bar{2}$0}, is smooth and crisscrossed by generally sharp and narrow polishing scratches. Fission tracks essentially appear as simple channels. The T-type sections, {10$\bar{1}$0} and {10$\bar{1}$1}, are characterized by a textured surface with few polishing scratches. As in the S-type section, etched fission tracks show up as simple channels. A similar distinction was made by Gleadow (1978) on the basis of observations of etched tracks in different surfaces of sphene. This distinction is also compatible with that made by Jafri et al. (1990) between hexagonal, pyramidal, and needle-type tracks in different surfaces of apatite, although both hexagonal and pyramidal tracks would indicate a P-type surface, whereas needle-type tracks would indicate either an S- or a T-type surface (probably S type, judging by the sharpness of the polishing scratches in Fig. 1E of Jafri et al. 1990). P-, S-, and T-type surfaces also exhibit quite different etching velocities (Table 1). It appears that the etching velocity perpendicular to the surface is lowest for P-type, intermediate for S-type, and highest for T-type surfaces. It follows that the slowest etching surfaces of apatite are not characterized by sharp polishing scratches (Gleadow 1981) but, instead, by broad flat-bottomed scratches.

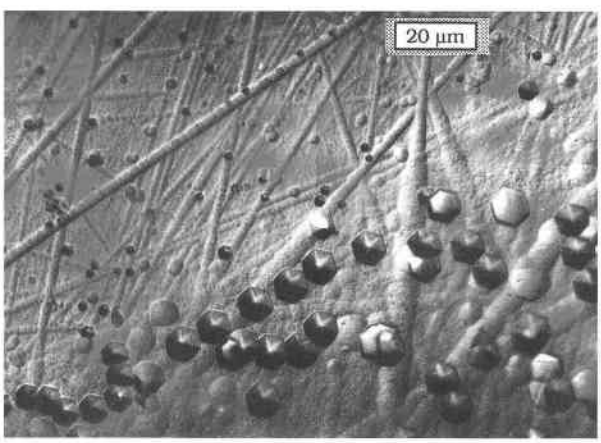

FIGURE 2. Contact between two regions of the {0001} surface (P type), etched for 60 s (top left) and 300 s (bottom right). There is almost no visible threshold between these two regions. Etchant concentration: 2.5% HNO_3 (set A).

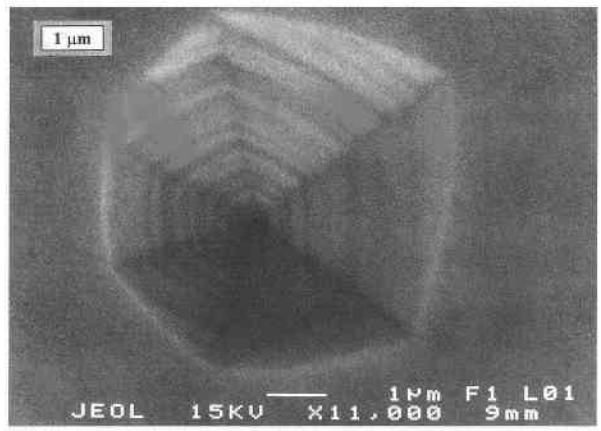

FIGURE 3. Etched dislocation in a P-type surface. Because the surface is at a slight angle to {0001}, the base of the etch pyramid is not a regular hexagon. The pyramid faces are terraced. The terraces are parallel to {0001}, as indicated by their regular hexagonal borders. The fact that the midpoints of these hexagons do not coincide indicates that the dislocation line is not exactly perpendicular to {0001}. Etching conditions: 25 s in 25% HNO_3.

P-type surfaces. After short etching time (60 s) the P-type surfaces are crisscrossed by broad, flat-bottomed polishing scratches, which gives them a considerably rougher appearance than the unetched surfaces (Fig. 2). The width of the scratches increases in proportion to etching time, whereas their depth remains virtually unchanged. As they overlap, the surface again becomes smoother in appearance, with only the deepest scratches remaining after 300 s. Shallow dishlike etch figures, similar to those ascribed by Gilman (1959) to clusters of point defects, were also observed on both P-type surfaces. Pointed etch pyramids situated at the emergence sites of isolated edge or screw dislocations, although common in many other apatites, are relatively rare in Durango apatite. Occasionally, the etch pyramids at dislocations are terraced (Fig. 3), as a result of interruptions in the etching process caused by impurities segregated along the dislocation (Gilman 1960). The terraces are parallel to {0001} and centered on the dislocation line. Rows of regularly spaced etch pyramids mark the boundaries between sections of the crystal with slightly different orientations (small-angle grain boundaries) (Lovell 1958). Depending on the coherence of the boundary, the distance between the constituent dislocations varies from values comparable to the lattice spacing to several micrometers. The former etch as quasi-continuous grooves with v-shaped cross sections, the latter as chains of isolated pyramids (Fig. 4). A quasi-continuous groove also develops around the edges of the P-type sections, along the contact between the crystal and

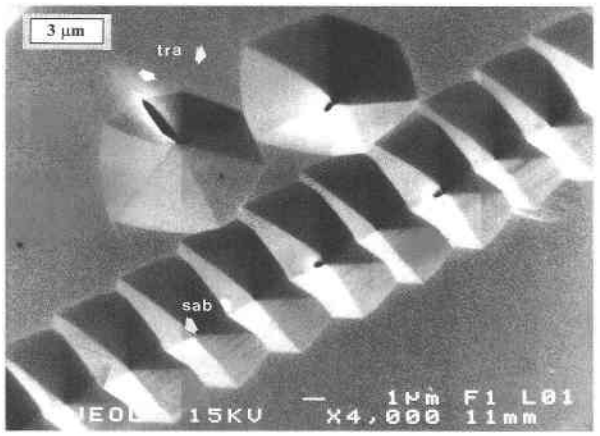

FIGURE 4. A row of partially overlapping, regularly spaced etch pyramids, marking a small-angle grain boundary (sab) in a cleaved P-type surface at a slight angle to {0001}. Two fission tracks (tra) are situated above the boundary. The surface is smooth because no defects were introduced by mechanical polishing. Etching conditions: 25 s in 25% HNO_3.

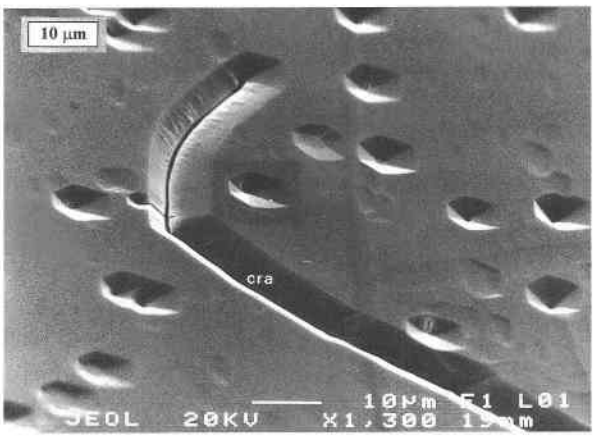

FIGURE 5. A continuous groove with v-shaped cross section along a crack (cra) in a cleaved P-type surface at a slight angle to {0001}. Etching conditions: 25 s in 25% HNO_3.

the surrounding epoxy resin, and along cracks intersecting the surface (Fig. 5).

Fission tracks are characterized by a typical funnel shape, consisting of an etch pyramid at the surface connected to a channel below (Fig. 6). Except for the influence of the track orientation, the pyramidal part is identical in shape and size to the etch pyramids at dislocations, grain boundaries, and cracks (Figs. 4 and 5). Its depth is not determined by the rate at which the etchant penetrates along the track because the etched track channels extend to depths considerably below that of the pyramids. The depth to which the etchant penetrates along a crack similarly exceeds that of the v-shaped groove at its intersection with the surface, as evidenced by the revelation of "tincles" (tracks in cleavage) at greater depth. Etch pyramids at dislocations, in contrast, are generally of the same depth as those at fission tracks or at cracks, although the etchant does not penetrate along the dislocation line. The formation and growth of etch pyramids is therefore not determined by the nature or properties of the defect, and in particular not by v_t (Wagner 1969; Somogyi 1980) in the case of fission tracks.

The etch pyramids on $\{11\bar{2}1\}$ have low symmetry and show a resemblance to etch figures observed by Honess (1927) and other features of the $\{11\bar{2}1\}$ surface described by Amelinckx (1955). The etch pyramid on {0001} is six sided, in accordance with the sixfold axis perpendicular to {0001} (Fig. 2). Its base, at the intersection with the surface, is a regular hexagon with slightly convex sides, approximately parallel to $\{2\bar{1}\bar{3}0\}$. Etch pyramids that develop at tracks at large angles (θ) to the surface are quite symmetric in the sense that their axis is parallel to the crystallographic c axis. Their depth is not noticeably influenced by θ. Asymmetric etch pyramids develop at tracks at smaller angles to the surface. In this case their depth decreases with decreasing θ. The faces above the opening to the track channels are reduced, whereas those opposite are enlarged, and the edges of the pyramid faces do not, then, intersect at a single point (Fig. 7; set A). The openings of tracks at glancing angles to the surface are shallow and not distinctly pyramidal in shape.

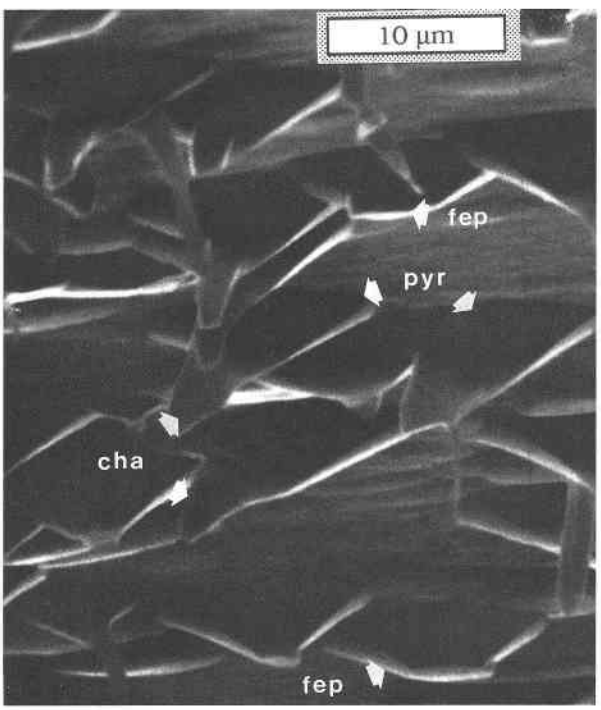

FIGURE 6. Funnel-shaped fission tracks in {0001} (P type). The etch pyramids (pyr) at the surface are connected below to etch channels (cha) that are mostly chisel shaped. Some of the shorter tracks are about to lose their etch channels and to turn into flat-bottomed etch pits (fep). Etching conditions: 300 s in 2.5% HNO_3 (set A).

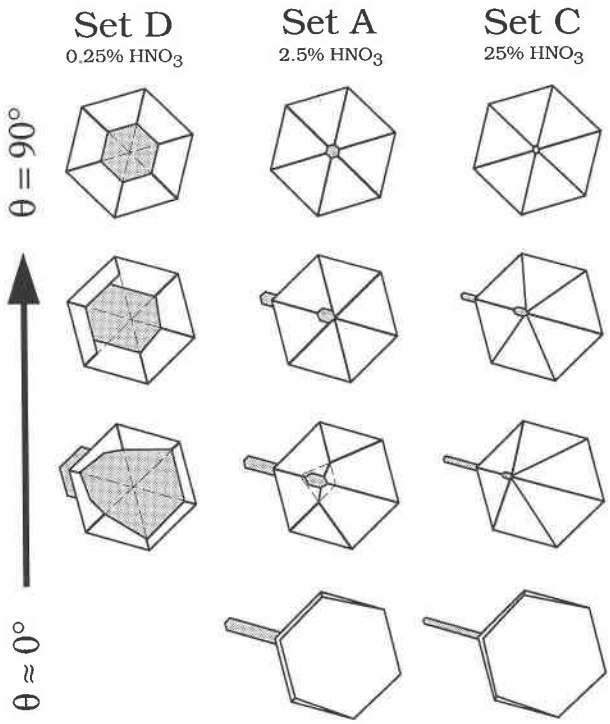

FIGURE 7. Diagram showing the etch-pyramid geometry in {0001} for different etchant concentrations. At high concentration (set C), the orientation of the pyramid faces is predominantly determined by the angle of incidence (θ) of the fission track, and their intersections meet at a single point along the track. At lower concentration (sets A and D), the orientation of the pyramid faces is less determined by θ than by crystal symmetry. Depending on θ, their intersections either do not meet at a single point (small θ) or do so at a point below the center of the hexagonal pyramid base (larger θ). The diagram also shows that the opening to the track channels (shaded areas) is situated to one side of the pyramid apex, and that the apparent channel width decreases with concentration.

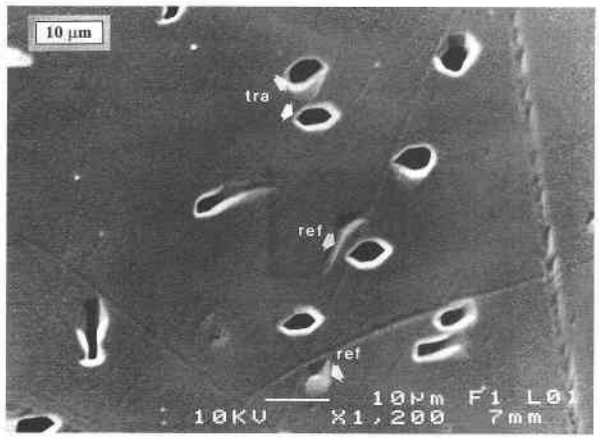

FIGURE 8. The $\{11\bar{2}0\}$ surface (S type), etched for 300 s in 2.5% HNO_3 (set A). The surface itself is comparatively smooth and crisscrossed by sharp polishing scratches. The track openings (tra) are essentially elongated hexagons, although the precise shape is often influenced by the orientation of the track. Some tracks develop minor additional structures at their intersection with the surface. Near the center of the image, a track at a slight angle to the surface is turning into a residual etch figure (ref). A fully developed residual etch figure (ref) is situated at the bottom of the photograph.

If a track is perpendicular to {0001}, then its etch channel is prismatic and bounded by planes approximately parallel to $\{21\bar{3}0\}$. Track channels in other directions are chisel shaped (Fig. 6). The projection of the track extremity onto {0001} is bounded by directions parallel to sides of the base of the etch pyramid. The length of the track channels decreases with etching time because the increase in the dimensions of the etch pyramids is not balanced by etching at the track extremities. The track channel disappears altogether when the pyramid overtakes the track extremity. At this stage, the etch pyramid becomes flat bottomed (Fig. 6), and its depth ceases to increase. Its diameter, however, continues to increase with etching time.

S-type surfaces. The S-type surface remains comparatively smooth after etching for up to 300 s (Fig. 8). After prolonged etching (1800 s) it becomes less smooth. Electron microscope images showed that the etched $\{11\bar{2}0\}$ surface is built of higher order prismatic planes. The relative width of their projections onto $\{11\bar{2}0\}$ suggests indices close to $\{21\bar{3}0\}$. Polishing scratches nearly parallel to the *c* axis are generally sharp and narrow. Scratches perpendicular to the *c* axis are generally broader and less sharp. The former, in particular, do not always terminate at the step that marks the contact between two regions of the apatite surface etched for a different length of time. Some scratches <1 μm deep continue uninterrupted when >10 μm of the apatite surface had been removed on one side (Fig. 9). No lattice defects identifiable as grain boundaries, isolated dislocations, or clusters of point defects were observed in the S-type surface. However, a few unknown defects, characterized by exceptional dimensions and preferential orientations, are present in all sections, including $\{11\bar{2}0\}$. The edges of the $\{11\bar{2}0\}$ section and cracks intersecting the surface show only minor signs of corrosion.

The fission tracks consist almost entirely of an etch channel, with only minor additional structures developing at their intersection with the surface (Fig. 8). The channel width observed through the microscope is smallest if the track projection onto the surface is either perpendicular or parallel to the *c* axis, and markedly larger in intermediate directions. The projection of the track extremities onto $\{11\bar{2}0\}$ is often characterized by directions approximately parallel and perpendicular to the *c* axis. The track population grows increasingly heterogeneous with etching time because of the addition of new tracks as a result of bulk etching. Newly added tracks are long and needlelike, whereas older tracks are shorter and broader (Fig. 10). This length difference arises because tracks below

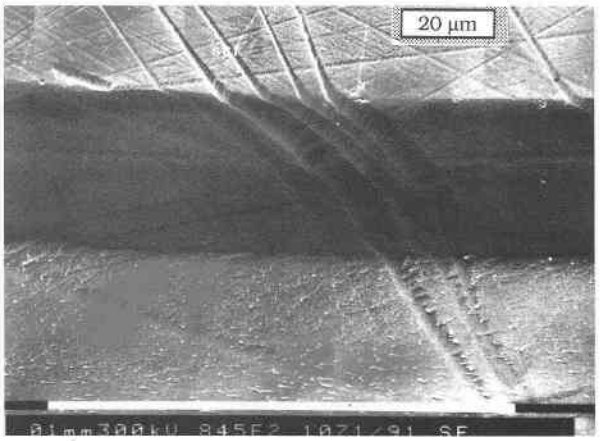

FIGURE 9. Contact between two regions of the {11$\bar{2}$0} surface (S type), etched for 60 s (top) and 1800 s (bottom). The height of the threshold between the two regions is approximately 11 μm. Some polishing scratches (scr) continue uninterrupted across the threshold, undergoing a small lateral displacement. Etchant concentration: 2.5% HNO_3 (set B).

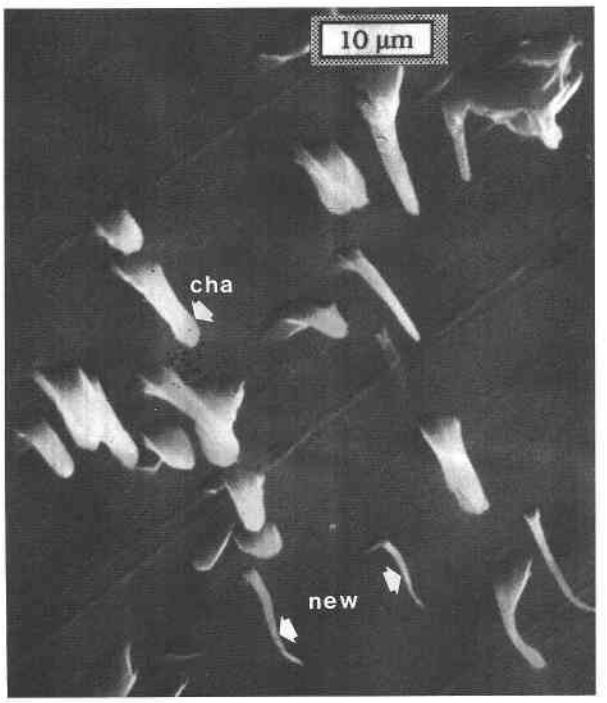

FIGURE 10. Chisel-shaped track channels (cha) in {11$\bar{2}$0} (S type) at intermediate concentration. The more needle-shaped channels correspond to tracks that were added as a result of bulk etching (new). Etching conditions: 300 s in 2.5% HNO_3 (set A).

the polished surface are on average longer than tracks intersecting it. There is, however, also a net decrease of the length of individual tracks with etching time because track shortening owing to etching of the surface is not balanced by an increase of track length owing to etching at the track extremity.

At etching times >120 s, envelopelike etch figures similar to those described by Honess (1927) develop on the S-type surface (Figs. 8 and 11). On {11$\bar{2}$0} most of these etch figures are approximately trapezoidal in outline and occur in a range of sizes. Their number and maximum size increase with etching time. They do not occur in alignments or clusters but have a random distribution like that of fission tracks. Partly for this reason, but mainly because of the occurrence of transitional forms (Fig. 8), they are considered as residual etch figures left by fission tracks. Tracks terminating within the layer removed by etching may thus leave an imprint in the surface when they cease to exist as etch channels. This is analogous to the observation that polishing scratches persist long after the layer containing the original defects has been etched away. Similar etch figures develop at the track openings after longer etching times (>120 s), although their development is strongly dependent on track orientation. In most cases only the prism plane at the side of the track opening opposite the track extremity is well developed. As a consequence, tracks with azimuthal angles between 0 and 180° with respect to the c axis show a liplike appendage on one side of the track opening, whereas those with azimuthal angles between 180 and 360° show a similar but more steeply inclined structure at the opposite side (Fig. 11), in agreement with the low hexagonal symmetry of apatite and in particular with the absence of mirror planes parallel to the c axis.

T-type surfaces. T-type surfaces are characterized by

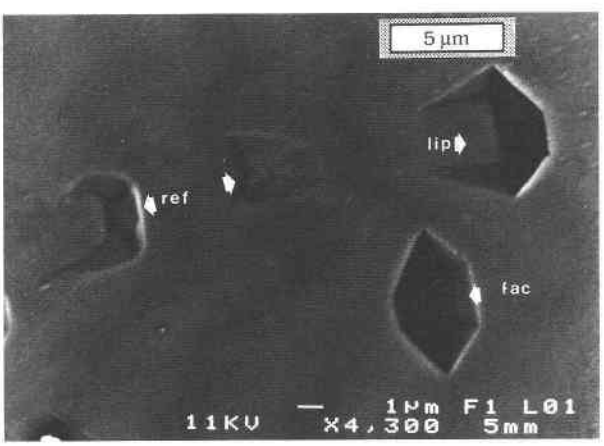

FIGURE 11. On the right, two tracks in {11$\bar{2}$0} (S type), showing the characteristic opening in the shape of an elongated hexagon with its long axis parallel to the crystallographic c axis. The upper track dips to the right and has a slightly inclined facet (lip) on the left-hand side of its opening. The lower track, which dips to the left, has a more steeply inclined facet (fac) on the opposite side. On the left, two residual etch figures (ref). Etching conditions: 300 s in 2.5% HNO_3 (set A).

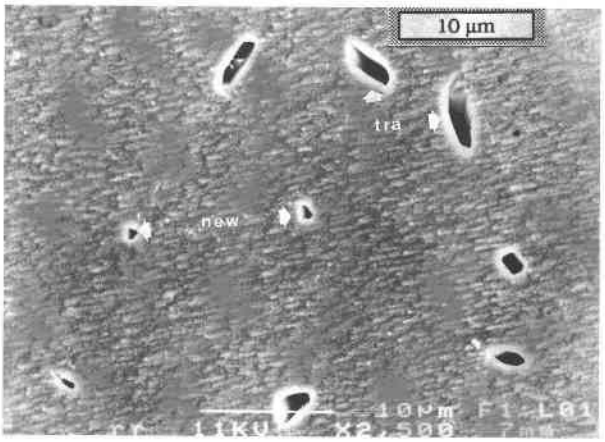

FIGURE 12. The openings of etched fission tracks (tra) in $\{10\bar{1}0\}$ (T type) are irregular and entirely lack the additional structures visible in P-type and, to a lesser extent, in S-type surfaces. The distinctly smaller openings (new) correspond to tracks that were added as a result of bulk etching. The characteristic texture of T-type surfaces is clearly discernable. Etching conditions: 300 s in 2.5% HNO_3 (set A).

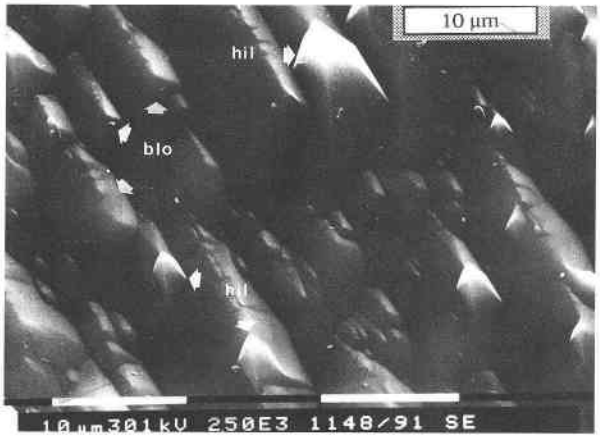

FIGURE 14. The texture on $\{10\bar{1}1\}$ (T type) is made up of two components. The fundamental texture has a blocklike aspect (blo) and is clearly distinguishable from the hillocks (hil) that make up the superimposed texture. There seems to be some spatial correlation between the two components. Etching conditions: 1800 s in 2.5% HNO_3 (set B).

a texture that grows coarser with each etching step (Fig. 12). After prolonged etching (1800 s) a basic texture and a superimposed texture can be distinguished. The basic texture on $\{10\bar{1}0\}$ consists of long asymmetric grooves and ridges with v-shaped cross sections parallel to the c axis (Fig. 13). Measurements of the relative widths of the projections of the faces making up these grooves and ridges onto $\{10\bar{1}0\}$ suggest indices close to $\{21\bar{3}0\}$. Similar measurements suggest that the basic texture on $\{10\bar{1}1\}$ (Fig. 14) consists of faces with indices close to $\{0001\}$ and $\{21\bar{3}0\}$. The superimposed texture on both $\{10\bar{1}0\}$ and $\{10\bar{1}1\}$ consists of fields of pyramidal hillocks that are usually closely spaced (Batterman 1957) (Figs. 13 and 14). Polishing scratches are relatively rare on T-type surfaces. Except for the ubiquitous defects, no other defects apart from fission tracks were revealed in the T-type surfaces. In particular, no etch figures were observed that could be identified as clusters of point defects, edge or screw dislocations, or small-angle grain boundaries. Neither the edges of the sections nor cracks intersecting the surface showed preferential corrosion by the etchant.

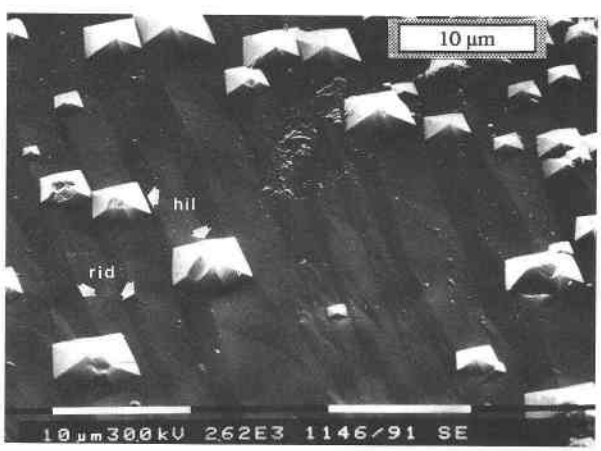

FIGURE 13. The texture on $\{10\bar{1}0\}$ (T type) is made up of two components. The fundamental texture consists of parallel ridges (rid) separated by grooves and is clearly distinguishable from the pointed hillocks (hil) that make up the superimposed texture. Etching conditions: 1800 s in 2.5% HNO_3 (set B).

Fission tracks consist entirely of an etch channel, with no distinct structures developing at their intersection with the surface (Fig. 12). After a short etching time, the channels are uniform in appearance, with no clear dependence of track width on orientation in either surface. Similar to the S-type surface, the track population grows increasingly heterogeneous after each etching step because of the addition of new tracks as a result of bulk etching. Newly added tracks are long and needlelike, older tracks shorter and broader. Contrary to the S-type surface, the tracks disappear without leaving a residual etch figure when the surface overtakes the track extremity. It was noticed, however, that the characteristics of an etched external $\{10\bar{1}0\}$ surface on a single crystal of Durango apatite do not agree with the description above but are similar to those of an S-type surface. It is therefore likely that the $\{10\bar{1}0\}$ sections used in these experiments are slightly off their desired orientation and that this affected their etching behavior. No such disagreement was observed for the other sections.

In summary, P-type, S-type, and T-type surfaces have certain contrasting properties that supersede the pragmatic distinctions made before. After a phase in which it acquires its initial roughness, a P-type surface grows smoother again with etching time. Any existing surface

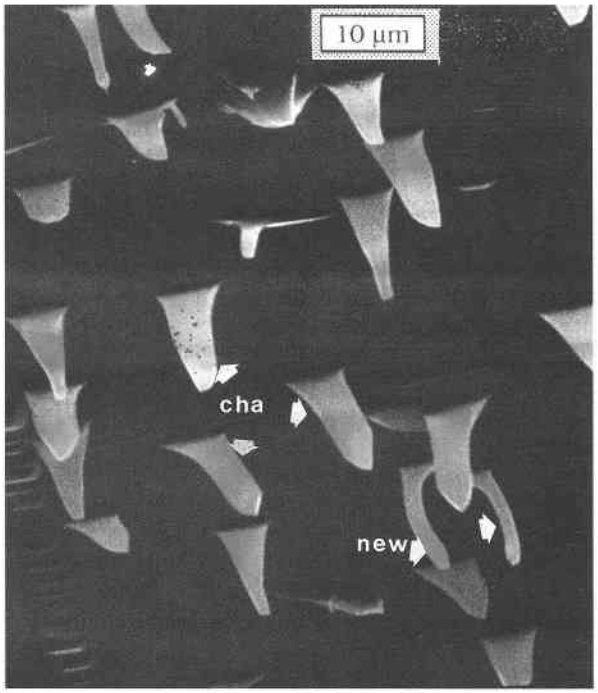

FIGURE 15. The track channels (cha) in $\{11\bar{2}0\}$ (S type) are characteristically knife-blade shaped at a high etchant concentration (25% HNO_3). The few distinctly narrower channels (new) correspond to tracks that were added as a result of bulk etching. Etching conditions: 60 s in 25% HNO_3 (set C).

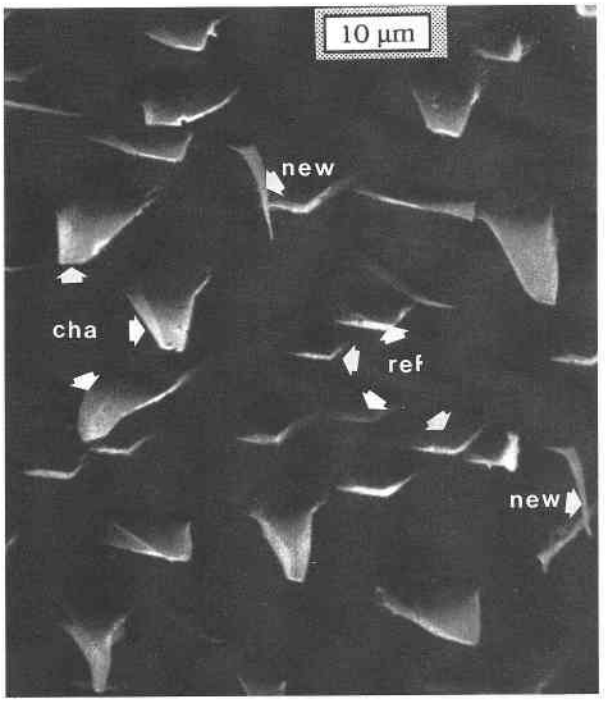

FIGURE 16. The track channels (cha) in $\{11\bar{2}0\}$ (S type) are nearly wedge shaped at a low etchant concentration (0.25% HNO_3). The needle-shaped channels (new) correspond to tracks that were added as a result of bulk etching. Residual etch figures (ref) are clearly developed at this concentration. Etching conditions: 1800 s in 0.25% HNO_3 (set D).

topography may eventually be entirely obliterated except for etch pyramids at fission tracks and other defects. An S-type surface remains comparatively smooth for long etching times, whereas a T-type surface develops a texture that grows progressively coarser. In neither of these are clusters of point defects, edge or screw dislocations, or small-angle grain boundaries revealed. An S-type surface has the remarkable property of retaining the signatures of fission tracks and polishing scratches long after the defects that originally gave rise to them have been removed. Although deep scratches in a P-type surface can also persist for some time, this is due to the low etch rate of the surface and not an intrinsic property.

Track geometry and etchant concentration

Increasing or decreasing the etchant concentration does not drastically alter the distinctive etching characteristics of the studied surfaces: {0001} retains the properties of a P-type surface and $\{11\bar{2}0\}$ those of an S-type surface throughout the range of concentrations employed. Etchant concentration does influence the details of track geometry in both {0001} and $\{11\bar{2}0\}$, however. Its effect on the track channels is most clearly observed in $\{11\bar{2}0\}$. At the highest concentration two of the channel walls are parallel to the c axis and much more developed than the others. Being parallel, with little separation between them, they confer a typical knife-blade shape on the tracks (Fig. 15). At intermediate concentration these walls are less developed and also further apart, which gives the track a chisel shape (Fig. 10). At the lowest concentration used, the track channels taper toward the track extremity and can be described as wedge shaped (Fig. 16). In $\{11\bar{2}0\}$, the separate structures that develop at the track openings become more prominent with decreasing concentration, ranging from a small collar at 25% HNO_3 (Fig. 15) to a structure akin to a small etch pyramid at 0.25% (Fig. 16). The residual etch figures in $\{11\bar{2}0\}$ are also more prominent at the lower concentration (Fig. 16).

At high concentration the axes of the etch pyramids on {0001} are approximately parallel to the track orientation. The pyramid faces intersect at a point the projection of which onto {0001} does not coincide with the center of the pyramid's hexagonal base, although it also never falls outside it (Fig. 7; set D). At low concentration most of the pyramid axes are parallel to the c axis. The pyramid faces intersect at a point below the center of the pyramid's hexagonal base (Fig. 7; set C). The pyramid geometry at intermediate concentration can be considered transitional between the geometries at low and high concentrations (Fig. 7; set A). The rate at which the maximum diameters of the etch pyramids in {0001} increase with etching time is also strongly influenced by concentration. Diameter measurements give the following values: 0.40(2) μm/min

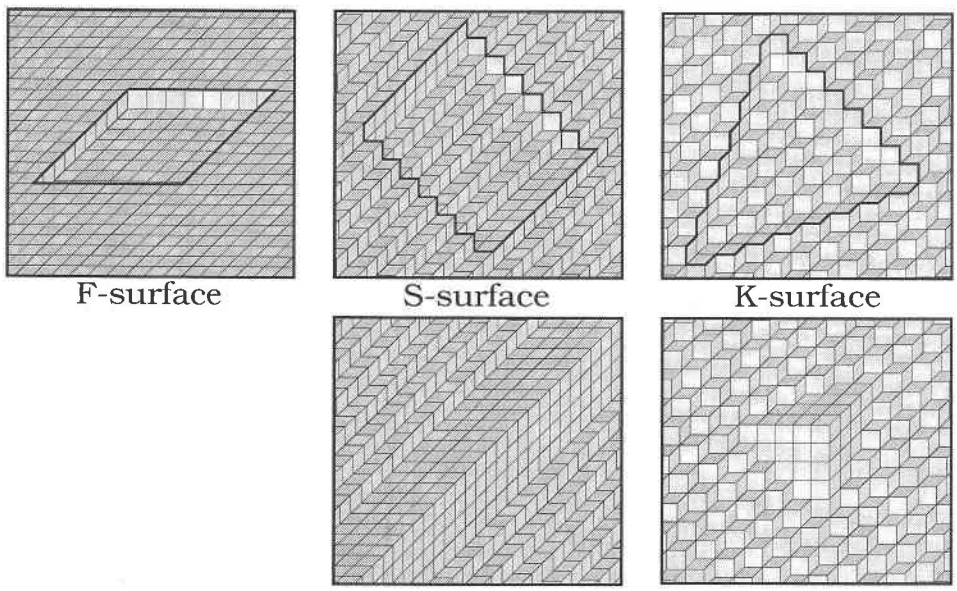

FIGURE 17. Top row: schematic representation of a two-dimensional nucleus in F, S, and K surfaces. Bottom row: building units assembled into macrosteps (S surface) and macrokinks (K surface).

for 0.25% HNO_3, 3.30(10) μm/min for 2.5% HNO_3, and 24.0(3) μm/min for 25% HNO_3.

INTERPRETATION

Basic approach

Our interpretation of these observations is based on concepts borrowed from the theories of crystal growth and dissolution. We consider two quite different approaches: an atomistic approach and a kinematic approach. The first treats growth and dissolution as phenomena involving the addition or removal of elementary building units to or from the crystal surface. The second treats growth and dissolution as geometric problems, involving the relative growth or dissolution rates of different crystallographic planes.

Atomistic approach. Following an atomistic approach we assume that etching proceeds by a succession of unit steps. Each step consists of the removal of an elementary building unit from the crystal surface. These units are bounded by edges parallel to the directions in which there is a continuous chain of strong bonds between the units. In the context of track revelation, the strong bonds are those that are most resistant to being broken by the action of the etchant upon the crystal lattice. They are analogous to the periodic bond chains in the atomistic theory of crystal growth and dissolution [Hartman 1973, 1978; Sangwal 1987; Bennema 1993; see also Terpstra et al. (1986) for apatite]. A given surface belongs to one of three categories, depending on its orientation with respect to the directions of the strong bonds: flat (F), stepped (S), or kinked (K). F surfaces are parallel to two or more strong bonds, S surfaces are parallel to one, and K surfaces are parallel to none (Fig. 17).

The removal of a building unit in a perfect F surface is known as nucleation. Considering only the interactions between nearest neighbors, the work of separation involved in nucleation may be represented by 5 E, where E corresponds to the work required to break a single bond (Gilman 1959). Nucleation causes the formation of a monomolecular pit. This alone is not sufficient to trigger the etching process because a monomolecular pit is thermodynamically unstable (Faust 1959). The dissolution of an F surface requires the formation of a two-dimensional nucleus. This profoundly affects the further dissolution of an F surface, which can then proceed by lateral displacement of the steps bordering the nucleus (Fig. 17). Following the principle of reciprocity, the nucleus is bounded by the steps with the lowest lateral shift velocities, i.e., the steps parallel to the directions of the strong bonds. The removal of a building unit from such a step requires 4 E. Because of thermal movements of the lattice, these steps are never perfectly straight but contain several kinks (Amelinckx 1964). The detachment of a building unit from a kink site requires only 3 E. The work of nucleation is also reduced at defects. The formation of a monomolecular pit at an edge dislocation, for example, requires only 4 E. Defects can therefore act as sites of preferential nucleation. Clusters of point defects may already constitute a nucleus. Linear defects extending into the volume of the crystal, such as fission tracks and dislocations, may guide the nucleation of successive lattice planes and lead to the formation of etch pyramids (Gilman 1959; Amelinckx 1964).

The removal of a building unit in a perfect S surface requires 4 E. Because of the presence of kinks in the surface steps, the formation of a two-dimensional nucleus is not required for dissolution. The formation of a nucleus is also of lesser consequence: The nucleus in Figure 17

is bounded by two edges that are parallel and two that are perpendicular to the direction of the strong bonds. The latter move apart parallel to the surface at an energy expenditure of 3 E per building unit removed. The edges parallel to the direction of the strong bonds are equivalent to surface steps. There is no mechanism that forces them apart. The nucleus must therefore grow in only one dimension. Thus, an observable etch pyramid need not develop at a defect intersecting an S surface. This is not to say that it cannot.

A building unit in a K surface is joined to three nearest neighbors. This is called a half-crystal position because three is one-half the number of neighbors of a unit within the volume of the crystal. The removal of a building unit in a half-crystal position promotes one or more of its neighbors to a half-crystal position. It is therefore a repeatable step. A two-dimensional nucleus in a K surface has no effect on dissolution because the configuration of building units remains essentially the same (Fig. 17). As a result, there is no mechanism for the formation of a visible etch pyramid at a defect intersecting a K surface.

Like crystal growth and dissolution, track revelation is considered to proceed essentially by the removal of the building units in half-crystal positions because it is both a repeatable step and requires the least energy expenditure per unit. This applies to F and S surfaces as well as to K surfaces. In an F surface it proceeds at kinks in the steps bordering a two-dimensional nucleus. In an S surface it proceeds at kinks in the surface steps and at the extremities of a one-dimensional nucleus. It occurs all over a K surface because all the building units are in half-crystal positions. Unless there are extraneous factors, the etching velocity perpendicular to the surface is determined by the availability of building units in half-crystal positions and therefore increases in the order of F, S, K.

Kinematic approach. This approach is based on the concept of a radial shift velocity, v_r (Frank 1958; Frank and Ives 1960). The radial shift velocity is a property of macroscopic surfaces and is represented by a vector normal to the surface, equal in magnitude to its rate of translation during dissolution. It is important to stress that v_r represents the rate of translation of a plane surface as a whole, whereas the bulk-etching velocity, v_b, on which the existing model for fission-track revelation in minerals is based, does not.

Two related principles derived from a kinematic approach are of interest to track revelation in apatite. The principle of reciprocity states that, upon dissolution, convex forms are bounded by fast etching planes and concave forms by slow etching planes (Batterman 1957). The converse holds for crystal growth. The cosine rule describes the trajectory of an intersection of two planes at an angle θ to each other, e.g., the crystal surface and a plane bounding an etch pyramid or a hillock. If the first has radial shift velocity v_{r0} and the second $v_{r\theta}$, then the locus of their intersection is a plane at an angle φ to the surface, where φ is given by $v_{r\theta} \sin \varphi = v_{r0} \sin (\theta + \varphi)$ (Irving 1962). If $v_{r\theta} = v_{r0} \cos \theta$, the intersection moves perpendicular to the surface ($\varphi = \pi/2$), and an etch pyramid or hillock neither grows nor shrinks (Fig. 18b). If $v_{r\theta} \neq v_{r0} \cos \theta$, then, depending on whether the intersection is convex or concave and whether $v_{r\theta} < v_{r0} \cos \theta$ or $v_{r\theta} > v_{r0} \cos \theta$, either the etch pyramid (or hillock) or the surface grows at the expense of the other (Figs. 18a and 18c).

An etch pyramid or hillock is stable only if its height and diameter do not decrease during dissolution. If either dimension decreases, the etch pyramid or hillock eventually disappears. The diameter of an etch pyramid increases if $v_{r\theta} > v_{r0} \cos \theta$ and decreases if $v_{r\theta} < v_{r0} \cos \theta$. Conversely, the diameter of a hillock decreases if $v_{r\theta} > v_{r0} \cos \theta$ and increases if $v_{r\theta} < v_{r0} \cos \theta$ (Figs. 18a–18c). In general, etch pyramids are therefore stable in slow etching surfaces and hillocks on fast etching surfaces. This agrees with the observation that etch pyramids are characteristic of P-type surfaces, which have the lowest radial shift velocities, and hillocks occur on T-type surfaces, which have the highest. It also follows that etch pyramids or hillocks can develop only if a suitable defect is present. Consider for example an etch pyramid. Any intersection of two planes bounding it is concave. According to the principle of reciprocity, the slowest etching planes would therefore develop. One of these is parallel to the surface because the etch pyramid itself is stable only in the slowest etching surfaces. Therefore, its height cannot increase unless a suitable defect prevents the plane parallel to the surface from developing at its apex. A similar argument holds for hillocks (Figs. 18d–18f).

The present interpretation of track revelation in apatite rests on the assumption that the pitted (P type), scratched (S type), and textured (T type) surfaces, distinguished on the basis of observations, correspond, respectively, to flat (F), stepped (S), and kinked (K) surfaces. This is supported by the fact that the radial shift velocities of P-, S-, and T-type surfaces fall into three distinct categories, with the lowest values corresponding to P-type, intermediate values to S-type, and the highest values to T-type surfaces. This constitutes a clear parallel with the order of etching velocities of F, S, and K surfaces expected on the basis of an atomistic approach. The fact that clusters of point defects, isolated edge and screw dislocations, and small-angle grain boundaries are revealed in the P-type surfaces, whereas no features attributable to these defects are observed in either the S- or T-type surfaces, also supports this interpretation.

Surface evolution

P-type surfaces. Mechanical polishing results in many dislocation loops in a thin surface layer (Buck 1959). Nucleation induced by these dislocation loops would account for the general roughness of P-type surfaces after relatively short etching times. Because of their limited depth, these dislocation loops are etched out after longer etching times. Because P-type surfaces are parallel to the displacement of the surface steps, any topography eventually disappears and the surface again acquires a smoother appearance. If a plot of etch-pyramid diameter against etch-

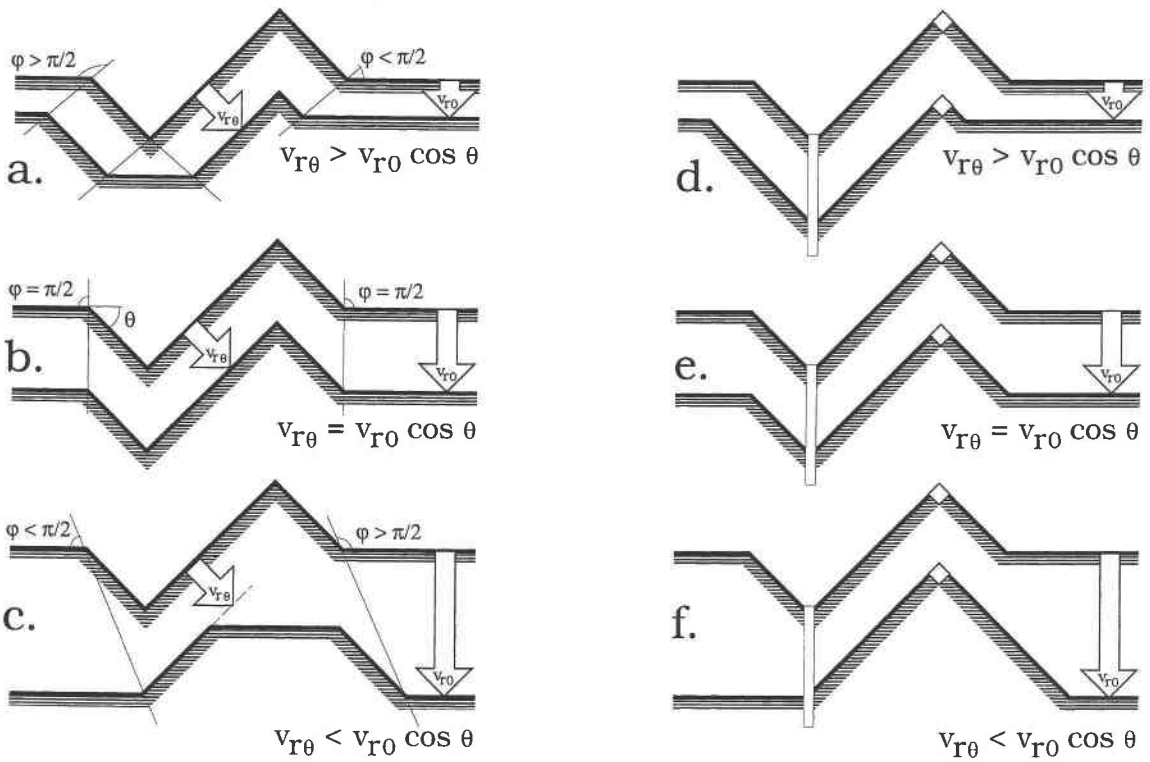

FIGURE 18. Diagram showing the evolution of a partially concave and partially convex feature bounded by planes at angle θ to the surface. (**a**) The diameter of the concavity increases and that of the convexity decreases in a slow etching surface ($v_{r\theta} > v_{r0} \cos\theta$); (**b**) if $v_{r\theta} = v_{r0} \cos\theta$, both diameters remain the same; (**c**) the diameter of the convexity increases and that of the concavity decreases in a fast etching surface ($v_{r\theta} < v_{r0} \cos\theta$). Height does not increase in either case, unless a suitable defect prevents the plane parallel to the surface from developing at their apex (**d–f**).

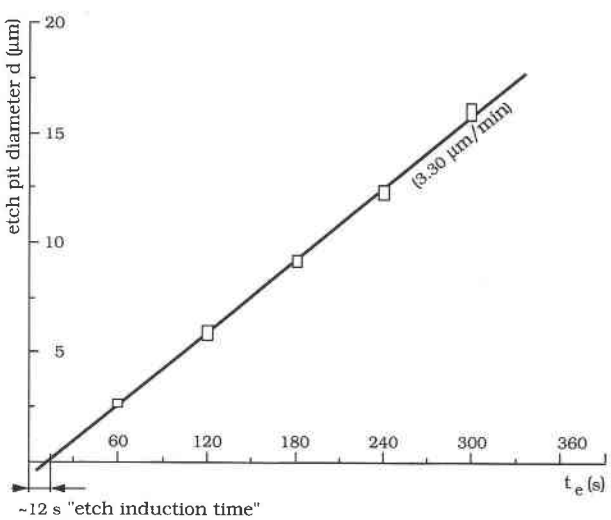

FIGURE 19. The evolution of the maximum diameter (d) of etch pyramids in {0001} (P type) as a function of etching time (t_e).

ing time (Fig. 19) is extrapolated to $t_e = 0$, it appears that there is an initial lag phase during which the diameter does not increase at the same rate. Although such lag phases are sometimes interpreted in terms of an etch induction time (Perron and Bourot-Denise 1986), it is perhaps more likely that they correspond to the interval during which the surface layer containing the dislocation loops is removed. There can indeed be no preferential nucleation at the intersection of a fission track or dislocation with the surface as long as it is riddled with dislocation loops. The etch pyramid diameter can therefore increase only after the dislocation loops have been removed by etching.

S- and T-type surfaces. Dislocation loops induced by polishing need not have the same effect on S- and T-type surfaces because their dissolution does not depend on nucleation. However, concentrations of dislocation loops extending deeper into the crystal, e.g., along polishing scratches, would appear in all surfaces. In contrast to the S-type surface, which, except for these scratches, remains essentially smooth for long etching times, the T-type surfaces show a progressively coarser texture, which is mainly due to the growth of hillocks. This can be understood in kinematic terms. The condition for hillock stability is $v_{r\theta} < v_{r0} \cos\theta$. The absence of hillocks on the

S-type surface would indicate that $v_{r\theta} > v_{r0} \cos \theta$, whereas their abundance on the T-type surfaces would indicate that $v_{r\theta} < v_{r0} \cos \theta$. This agrees with the observation that the S-type surface is characterized by a lower radial shift velocity than the T-type surfaces.

Figure 17 shows how the basic textures on S- and T-type surfaces of apatite could consist of building units assembled into "macrosteps" and "macrokinks," respectively, as proposed by Franke et al. (1975) and Heimann et al. (1975) for macrokinks observed on the faces of the dissolution forms of silicium, germanium, and periclase crystals. There are two problems with this interpretation. First, the atomistic approach provides no mechanism for developing macrosteps or macrokinks on an initially flat surface. Second, convex projections bounded by the relatively slow etching F faces are theoretically unstable according to the principle of reciprocity. According to Franke et al. (1975) and Heimann et al. (1975), however, the intersection of two or more F faces has some stability, which explains why macrokinks can exist at all. Their stability must, however, be limited because the dissolution forms of crystals are never seen to be made up of F faces on a macroscopic scale. The growth of hillocks is generally ascribed to impurities that locally inhibit dissolution (Batterman 1957). When stable, macrokinks or macrosteps could equally well accommodate these impurities, which would account for their growth. However, they must collapse at some point because of their limited stability. A new convexity, not bounded by F faces but by a kinematically stable configuration of fast etching planes, i.e., a conventional hillock, must then develop to accommodate the impurity. This offers a simple explanation for the observation that the texture of T-type surfaces is made up of two distinct sets of convex projections, one of which at least must violate the principle of reciprocity. At the same time it accounts for the roughly comparable dimensions of hillocks and macrokinks (and the width of macrosteps) and for the fact that hillocks frequently seem to be positioned on top of a macrokink or astride a macrostep (Figs. 13 and 14).

We have mentioned an inconsistency in our observations: The $\{10\bar{1}0\}$ surface was identified as type T because of its high radial shift velocity and the presence of hillocks. Its basic texture, however, consists of macrosteps and implies type S. It also follows that, because the steps on $\{11\bar{2}0\}$ are parallel to the c axis, the apatite lattice has a strong bond chain parallel to this axis. This, in turn, implies that all prismatic faces, including $\{10\bar{1}0\}$, must be either S or F surfaces, corresponding to the S or P type, respectively. It was concluded earlier that the $\{10\bar{1}0\}$ sections were possibly slightly off their desired orientation, and that this resulted in a deviation from their true etching behavior. A repeat experiment designed to check this inconsistency confirmed that $\{10\bar{1}0\}$ is actually characterized by sharp polishing scratches and is therefore of type S. Triangular residual etch figures, similar to those described by Honess (1927), were observed on this $\{10\bar{1}0\}$ section. At a concentration of 2.5% HNO_3, the fission tracks consisted essentially of an etch channel with only minor additional structures developing at their intersection with the surface.

Track revelation

The track channel. Because the track channels are etched over their entire length even after a short etching time, it is evident that the track-etching velocity, v_t, is high in comparison with the etching velocity of the undamaged material. The experiments reported here did not allow the measurement of v_t. The most accurate values reported to date were probably obtained by the etch-anneal-etch method (Green et al. 1978; Belyaev et al. 1988). These values indicate that v_t exceeds the etching velocity of the undamaged material by at least two orders of magnitude in orthopyroxene and muscovite. It is reasonable to assume that this is also true for apatite. The etching time necessary for tracks to become visible under the optical microscope is then essentially determined by the rate of increase of their channel width.

Track channels are concave and therefore bounded by the slowest etching planes according to the principle of reciprocity. This can be the case only up to a point because the etched channels must follow the track axis. Two of the walls of the tracks in the $\{11\bar{2}0\}$ section are clearly also parallel to the crystallographic c axis. These walls, therefore, contain no kinks, except for those created by thermal movements of the lattice, but consist entirely of steps parallel to the c axis. The other channel walls are kinked surfaces, unless the track axis is either parallel or perpendicular to the c axis. The assumption that stepped surfaces etch more slowly than kinked surfaces would therefore account for the flattened shape of most track channels. Our observations also confirm that tracks parallel and perpendicular to the c axis are narrower and deviate from the chisel shape.

It is generally accepted that v_t falls off abruptly at a point along the track where the lattice damage drops below a certain threshold, and that any further increase of track length occurs at a rate, v_e, determined by the etching velocity of the undamaged crystal. In contrast to the etch channel, where track orientation imposes a restriction on the planes that can constitute the channel walls, no such restriction exists at the track extremities. Following the principle of reciprocity, these extremities are therefore bounded by the slowest etching planes, i.e., F planes. If the fission damage beyond this point is discontinuous or otherwise insufficient to cause nucleation of the planes intersecting there, v_e would be very small. There is some evidence in support of this. The dishlike etch figure that is left where an etch pyramid in a P-type surface has overtaken the track extremity does not have a pointed bottom but a perfectly flat one. It is therefore concluded that virtually no nucleation takes place at the track extremities, and that $v_e = 0$.

Green et al. (1986) observed that the lengths of horizontal confined tracks in Durango apatite, etched in 5 M HNO_3, showed no significant increase when etching time

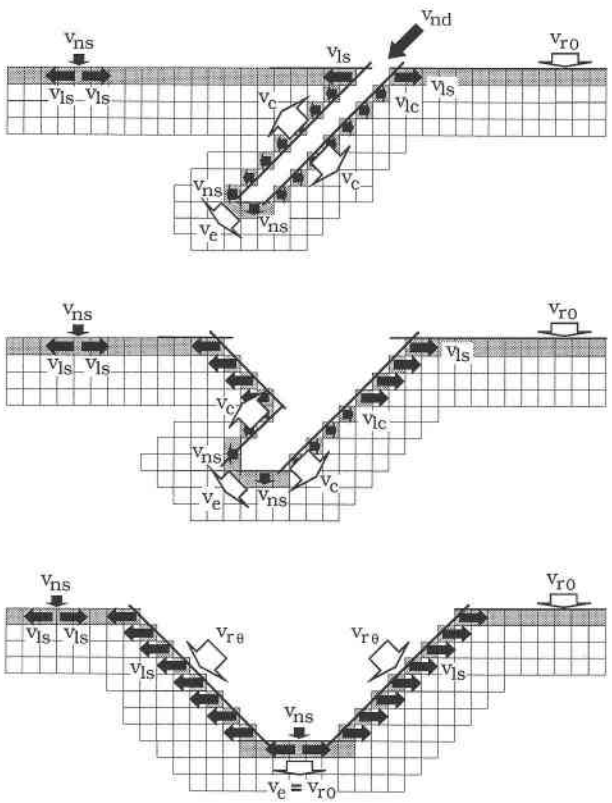

FIGURE 20. Schematic representation of track revelation, from top to bottom, in a P-type surface. Black arrows (atomistic approach) = nucleation velocity of the intact surface (v_{ns}), velocity at the point of intersection of a defect (v_{nd}), lateral shift velocity of surface steps (v_{ls}), and lateral velocity along the track core (v_{lc}). White arrows (kinematic approach) = radial shift velocity of the surface (v_{r0}), the channel walls (v_c), etch-pit faces ($v_{r\theta}$), and the etching velocity at the track extremity (v_e).

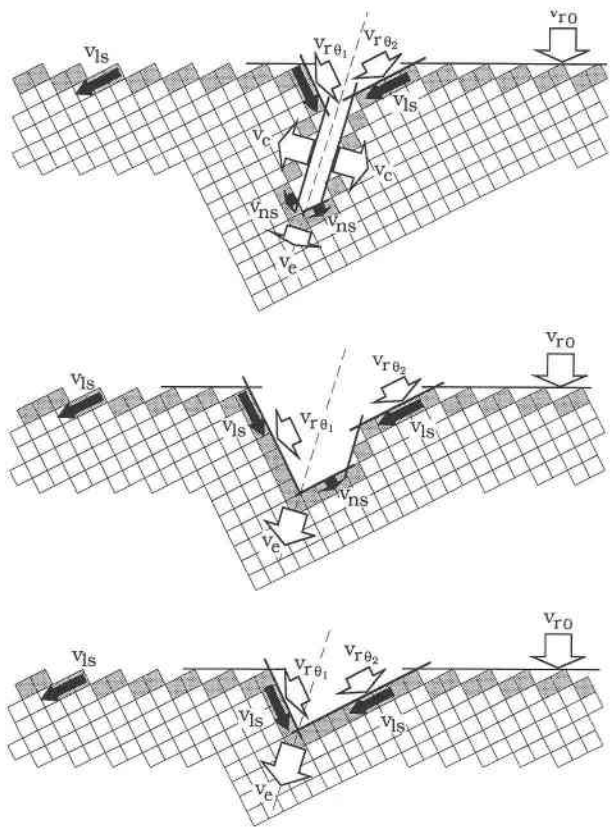

FIGURE 21. Schematic representation of track revelation in an S-type surface. The etching velocities are the same as in Figure 20. Note that v_e increases if the F planes bounding the track extremity become exposed at the surface (bottom). This stage can also represent the evolution of a polishing scratch parallel to the c axis.

was increased from 20 to 50 s in 10 s steps. They concluded that a population of newly etched confined tracks was measured after each etching step, obscuring any real increase of track length with etching time. This conclusion is difficult to reconcile with the fact that newly etched confined tracks are less likely to be observed under the microscope than older tracks (Green et al. 1986). An alternative explanation, suggested by the track-revelation mechanism proposed here, holds that the length of confined tracks actually does not increase significantly.

The length of individual surface tracks decreases with etching time. In P-type surfaces this is mainly due to the increasing dimensions of the etch pyramids (Fig. 20). In S- and T-type surfaces this results from the relatively high radial shift velocity of the surface itself (Fig. 21). However, just before the surface overtakes the track extremity the F planes bounding it are exposed at the surface. At this point their radial shift velocity increases because they no longer require nucleation. This increase may be sufficient to satisfy the kinematic condition for stability, i.e., $v_{r\theta} > v_{r0} \cos \theta$. If so, a fission track leaves a residual etch figure regardless of the thickness of the apatite layer removed by dissolution. If not, the track disappears completely. Our observations show that residual etch figures left by fission tracks are stable in the S-type surface but not in the T-type surfaces of apatite, in general agreement with the conclusion, based on the occurrence of hillocks, that $v_{r\theta} > v_{r0} \cos \theta$ for the S-type surface and $v_{r\theta} < v_{r0} \cos \theta$ for the T-type surfaces. This argument also makes it clear why polishing scratches remain visible in S-type surfaces when the thickness of apatite removed during etching exceeds the depth of the scratches by more than an order of magnitude, and why polishing scratches in T-type surfaces are rare and indistinct even after relatively short etching times. According to the mechanism shown in Figure 21, the displacement of a scratch is not exactly perpendicular to the surface but at an angle determined by its orientation relative to the F planes. This is confirmed by our observations (Fig. 9).

The etch pyramid. Defects determine the sites at which etch pyramids develop by acting as catalysts for nucleation. Many defects may serve this purpose although neither their nature nor their properties, e.g., v_t in

the case of fission tracks, influence the velocity of nucleation (v_{nd} as opposed to v_{nd}, the nucleation velocity of the undamaged surface) or the lateral shift velocity of the surface steps (v_{ls}). Because identical etch pyramids are situated at the intersection of a dislocation, fission track, etc., with the crystal surface, their development must be entirely governed by the properties of the surface.

Lacmann et al. (1974) calculated that the lateral shift velocity of steps increases rapidly with interstep spacing (δ) for small values of δ, and reaches a constant value above a certain limit, δ_l. If a similar relation holds for the dissolution of apatite in nitric acid, the geometry of etch pyramids in P-type surfaces may be better understood. It is convenient to consider just two velocities: v_{lc} for $\delta < \delta_l$ and v_{ls} for $\delta > \delta_l$. Steps on the surface move laterally at velocity v_{ls}, whereas steps in the underlying lattice planes, e.g., along the core of a fission track, move at the lower velocity, v_{lc}. When the surface steps have moved away a distance δ_l from the nucleus in the underlying lattice plane, the latter acquires the characteristics of a surface and, accordingly, v_{lc} increases to v_{ls}. After twice that time, steps in the third lattice plane acquire the lateral shift velocity of surface steps, and so on. This implies that the planes bounding an etch pyramid can have no greater inclination to the surface than an angle, ω, given by $\tan \omega = \epsilon/\delta_l$, where ϵ represents the step height. The velocity of nucleation along a linear defect can be represented by a vector parallel to the defect, which can be split into a component parallel (v_{ndp}) and perpendicular (v_{ndn}) to the surface. In the present case, in which etch-pyramid development is a surface-controlled process, v_{ndn} is constant for fixed etching conditions. The following cases can then be distinguished, depending on the values of v_{ls}, v_{ndn}, and ω, and on the angle of incidence, θ, of the fission track: (1) $\tan \omega > v_{ndn}/v_{ls}$ (Fig. 22a): (a) $\theta = 90°$, the pyramid axis coincides with both the t axis and the c axis (Fig. 22c); (b) $\tan \theta > v_{ndn} \tan \omega/(v_{ls} \tan \omega - v_{ndn})$, the pyramid axis coincides with the t axis but not with the c axis (Fig. 22e); (c) $\tan \theta < v_{ndn} \tan \omega/(v_{ls} \tan \omega - v_{ndn})$, the pyramid axis coincides with neither the t axis nor the c axis (Fig. 22g); (2) $\tan \omega < v_{ndn}/v_{ls}$ (Fig. 22b): (a) $\theta = 90°$, the pyramid axis coincides with both the t axis and the c axis (Fig. 22d); (b) $\tan \theta > v_{ndn} \tan \omega/(v_{ndn} - v_{ls} \tan \omega)$, the pyramid axis coincides with the c axis but not with the t axis (Fig. 22f); (c) $\tan \theta < v_{ndn} \tan \omega/(v_{ndn} - v_{ls} \tan \omega)$, the pyramid axis coincides with neither the c axis nor the t axis (Fig. 22h).

This hypothesis has several interesting consequences. First and foremost, it allows for such different factors as crystal symmetry and track orientation to control pyramid geometry at different concentrations. At the highest concentration used (set C) the observed dependence of pyramid geometry on track orientation is consistent with 1, whereas at low (set D) and intermediate (set A) concentrations it is more consistent with 2. For these observations, it is sufficient that the v_{ls}/v_{ndn} ratio increases with concentration. Although this was not established by measurement, it was observed that v_{ls} increases rapidly with concentration. Second, the hypothesis accounts for the observation that etch pyramids never undercut the surface and that the openings to the track channels do not connect directly to the pyramid apex but instead are situated to one side in one of the pyramid faces. Third, it explains why, for large values of θ, the depth of the pyramids is independent of θ, whereas for smaller values of θ depth decreases steadily. Fourth, it accounts for the fact that for small values of θ, the edges bounding the pyramid faces cease to intersect at one point and that at the same time the faces above the opening to the track channel are reduced, whereas those opposite are enlarged. Fifth, it explains why the terraces occasionally observed on the faces of etch pyramids at dislocations are parallel to a known F surface, i.e., {0001}. Interruptions of the nucleation process, because of impurities segregated along the dislocation line, account for the formation of the terraces themselves. More generally, this hypothesis explains why pyramid diameter and depth are usually the same at dislocations, fission tracks, etc., and independent of the true rate of penetration of the etchant.

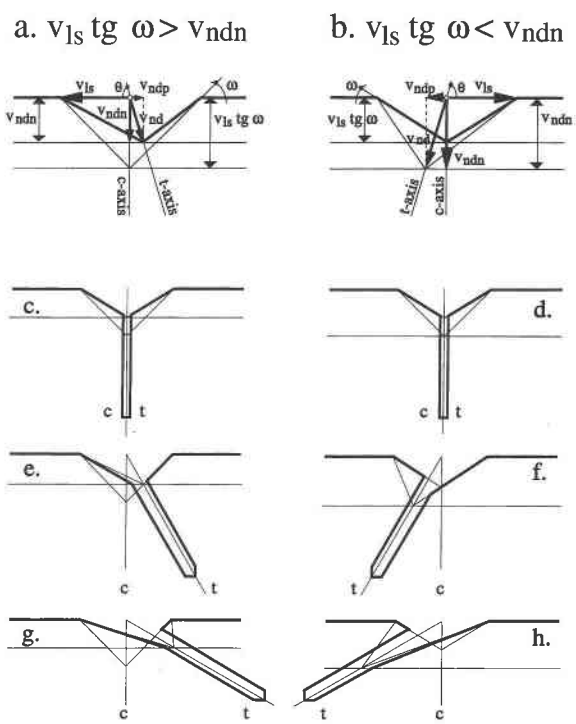

FIGURE 22. Diagram showing different etch-pit profiles in {0001}, depending on the values of v_{ls}, v_{ndn}, and ω and on the angle of incidence, θ, of the fission track; (**a**) $\tan \omega > v_{ndn}/v_{ls}$, (**b**) $\tan \omega < v_{ndn}/v_{ls}$, (**c**) $\theta = 90°$, (**d**) $\theta = 90°$, (**e**) $\tan \theta > v_{ndn} \tan \omega/(v_{ls} \tan \omega - v_{ndn})$, (**f**) $\tan \theta > v_{ndn} \tan \omega/(v_{ndn} - v_{ls} \tan \omega)$, (**g**) $\tan \theta < v_{ndn} \tan \omega/(v_{ls} \tan \omega - v_{ndn})$, (**h**) $\tan \theta < v_{ndn} \tan \omega/(v_{ndn} - v_{ls} \tan \omega)$.

Etchant concentration

The limited observations on the basis of the present experiments indicate a general leveling of etching veloc-

TABLE 2. Density (ρ_s; 10^5/cm^2) of spontaneous tracks in different crystallographic planes of Durango apatite as a function of etching time (t_e; s)

Section	Type	ρ_s	[t_e = 60]	s/s_P	ρ_s	[t_e = 120]	s/s_P	ρ_s	[t_e = 180]	s/s_P	ρ_s	[t_e = 240]	s/s_P	ρ_s	[t_e = 300]	s/s_P
Analyst 1 (R.J.)																
{0001}	P	2.11(5)	(2611)	1.09	1.99(4)	(2455)	0.97	1.90(4)	(2400)	0.95	1.83(4)	(2255)	0.94	1.73(4)	(2168)	1.03
{11$\bar{2}$1}	P	2.08(6)	(1344)	0.89	2.00(5)	(1561)	0.96	1.96(6)	(1208)	0.95	1.91(6)	(1178)	1.04	1.83(6)	(1127)	0.92
{11$\bar{2}$0}	S	1.96(4)	(2413)	1.07	2.47(5)	(3047)	1.04	2.76(5)	(2674)	1.04	2.89(5)	(2225)	0.95	2.96(5)	(2084)	0.99
{10$\bar{1}$0}	T	2.08(6)	(1279)	1.09	1.85(6)	(1138)	0.96	1.89(6)	(1185)	0.99	2.00(6)	(1231)	0.92	1.97(6)	(1214)	1.00
{10$\bar{1}$1}	T	1.80(6)	(1095)	1.06	1.85(6)	(1149)	1.10	1.91(6)	(1409)	1.11	2.03(6)	(1253)	1.01	2.01(6)	(1253)	1.13
Analyst 2 (P.V.)																
{0001}	P	1.96(6)	(1205)	1.05	1.86(6)	(1098)	1.01	1.84(5)	(1135)	0.99	1.64(5)	(1011)	0.92	1.51(4)	(932)	0.89
{11$\bar{2}$0}	S	1.86(5)	(1321)	0.97	2.06(5)	(1459)	0.97	2.02(5)	(1482)	0.94	2.19(5)	(1564)	1.06	2.25(5)	(1666)	0.93
{10$\bar{1}$0}	T	1.90(5)	(1465)	1.08	1.83(5)	(1237)	1.04	1.82(5)	(2021)	1.11	1.80(5)	(1290)	1.02	1.97(5)	(1332)	0.94

Note: Data for set A: 2.5% HNO_3, 25 °C. Errors are quoted at the 1σ confidence level. The number of tracks counted is given in brackets; s/s_P represents the ratio of the standard deviation of the track-density distribution to that of the Poisson distribution.

ities with decreasing concentration, as evidenced by the channel cross sections evolving toward more equidimensional shapes and by a lowering of the ratio of etch-pyramid diameters to channel widths in {0001}. This suggests that other factors besides the intrinsic surface properties influence the etching velocities at low concentration. Diffusion of the etchant and reaction products to and from the reaction sites is one possible factor. According to Irving (1962), diffusion control reduces the highest radial shift velocities without affecting the lowest. This accounts for the more uniform track dimensions at lower concentration. Consider also the cosine condition for additional faces to develop at a track intersection with an S-type surface (Fig. 21): $v_{r\theta} > v_{r0} \cos \theta$. Without diffusion control, $v_{r\theta 1}$ and $v_{r\theta 2}$, both relating to F surfaces, are small in comparison with v_{r0} and would not satisfy the condition for growth. With diffusion control, the difference between $v_{r\theta 1}$, $v_{r\theta 2}$, and v_{r0} decreases and the value of θ becomes relevant. In general, this implies that tracks become bounded by additional faces as etchant concentration decreases. More specifically, it accounts for the greater prominence of residual etch figures and separate structures at the track openings in {11$\bar{2}$0} at low concentration. Etching time and etchant concentration are therefore not interchangeable, and the choice of a suitable concentration merits careful consideration. A high concentration seems preferable for the purpose of apatite fission-track analysis. It prevents the development of interfering structures at the track openings in the prism faces and reduces the problem of residual etch figures. On the other hand, the optimum etching time decreases with concentration and becomes less reproducible.

Track densities

Measurements. The variability of track shapes makes it difficult to apply exactly the same track-determination criteria to P-, S-, and T-type surfaces. Tracks were only counted as such in the P-type surfaces if, besides an etch pyramid, they also showed a distinct etch channel. In the S-type surface, all straight, channel-like etch figures were counted as tracks unless characterized by an abnormal length or preferential orientation. Analyst 1 also included the envelope-shaped residual etch figures in his track counts. Analyst 2 did not count these as tracks. Because no residual etch figures were observed in the T-type surfaces, both analysts adopted the same criteria, counting only straight channellike etch figures as tracks, excluding those characterized by an abnormal length or preferential orientation. The track densities are reported in Table 2. The standard deviations of the density distributions (s) are close to the values for a Poisson distribution (s_P), suggesting that U is approximately homogeneously distributed. Because the s/s_P ratios provide only a fairly insensitive measure of the heterogeneity of the U distribution, s/s_P ratios close to 1 do not imply the absence of any U heterogeneity in Durango apatite.

After etching for 60 s, the track densities in the different sections are approximately the same. The track densities reported by analyst 2 for {0001}, {11$\bar{2}$0}, and {10$\bar{1}$0} are identical within the limits of statistical uncertainty. This is also the case for the track densities reported by analyst 1, except for the lower value recorded for the {10$\bar{1}$1} section. The difference between {10$\bar{1}$1} and all the other sections is statistically significant at the 99% confidence level. The differences between {0001}, {11$\bar{2}$0}, {10$\bar{1}$0}, and {11$\bar{2}$1} could be ascribed to Poisson variation, with the possible exception of the difference between {0001} and {11$\bar{2}$0}, which is significant at the 95% level but not at the 99% level. However, Poisson variation need not be the only factor responsible for the observed track-density differences. As argued above, U heterogeneity between the sections cannot be ruled out entirely as a contributing factor. Additional variation may also result from unsteady track-determination criteria, which may result from the different track geometries in different types of sections but also from subjective factors proper to the analyst. Except for U heterogeneity, subjective factors best explain the significant track-density difference between both T-type sections, reported by analyst 1. Considering these additional sources of variation, it is fair to conclude that the actual track densities are approximately the same in P-, S-, and T-type sections of apatite at etching times relatively close to the limit of track revelation.

The evolution of track density with etching time in P-, S-, and T-type sections of apatite is characterized by a distinctive trend (Fig. 23). The track density in both P-type sections decreases with etching time. The track density in the S-type section, in contrast, increases with etching time. Both analysts differ considerably, however, as to the magnitude of this increase because of their different track-determination criteria. The trend for T-type surfaces is less clear, although both analysts observed a trend intermediate between those for P- and S-type surfaces.

P-type surfaces. The track-density decrease in both P-type surfaces can be understood as a consequence of the increasing dimensions of the etch pyramids. As a result, a steadily increasing number of tracks are consumed by their etch pyramid. At this point, they lose their characteristic funnel shape and are no longer counted as tracks. The observed decrease is therefore a consequence of the track-determination criteria. As such, it is influenced by the track geometry and by the analyst. This accounts for the observation that the rate of track-density decrease is different for both P-type sections and also depends on the analyst.

T-type surfaces. In relation to the track-density evolution in both T-type surfaces, two competing factors must be considered: Although some tracks are lost as the surface overtakes the track extremities, tracks newly exposed at the surface are added to the population. The number of tracks added in this way exactly balances the number of tracks lost, so the track density is theoretically independent of etching time. However, the track population grows increasingly heterogeneous with etching time because the effective length of time for which the individual tracks have been etched ranges from zero for newly added tracks to the total submersion time for tracks intersecting the polished surface. The average track geometry thus evolves with etching time, thereby allowing the track-determination criteria to interfere with the track counts. This accounts for the slightly different trends observed by both analysts. Both analysts agree, however, that track density remains fairly constant in the T-type surfaces of apatite.

S-type surfaces. The same argument applies to the S-type surface, except that tracks overtaken by the surface leave a residual etch figure. Analyst 2, who did not include these tracks in his counts, observed a track-density increase of ~21% between t_e = 60 s and t_e = 300 s, or ~5% per 60 s etching step. Analyst 1, who did include the residual etch figures in his track counts, observed a total increase of ~51%, or ~25% over and above the expected increase (approximately 26% for v_r = 0.37 μm/min and a total track length of 14.4 μm). Although it seems unlikely that these trends result from the interplay between the changing track morphology and the track-determination criteria, it is hazardous to venture an alternative explanation without further verification. The possibility of a real increase in the density of etched fission tracks with etching time in S-type surfaces of apatite may merit consideration. Although no mechanism can at present be put forward to account for this, the possibility should not be discarded prima facie. The interactions between the crystal surface, the damage left by the fission fragments, and the etchant have proved more complicated than expected.

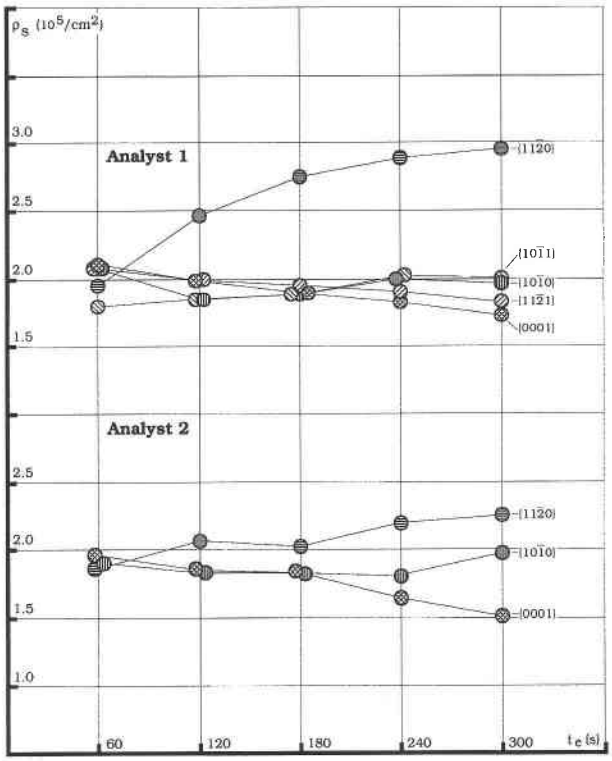

FIGURE 23. Evolution of the spontaneous track density (ρ_s) in the {0001}, {10$\bar{1}$0}, {11$\bar{2}$0}, {10$\bar{1}$1}, and {11$\bar{2}$1} sections of Durango apatite as a function of etching time (t_e). The diameter of the circles corresponds to a 1σ error interval.

CONCLUSIONS

A model of track revelation in minerals is of considerable interest to fission-track analysts. It would be particularly helpful in understanding the factors that determine track-etching efficiency and influence track-length measurements. A valid model must account for the complex track geometries observed in minerals and their dependence on surface orientation. The classic two-component (v_b-v_t) model fails in these respects. It is also fundamentally at variance with the kinematic theory of crystal growth and dissolution, in which growth and dissolution velocities are considered vector properties of crystallographic planes.

A model, such as considered by Maurette (1966), based on radial shift velocities instead of bulk-etching velocities, provides an alternative to the v_b-v_t model. Moreover, if v_t is high in comparison with v_r, its actual value is unimportant, and it becomes possible in principle to calculate track geometries on the basis of the radial shift velocities alone. The theoretical framework for such cal-

culations was developed by Frank (1958), and a related method was reported by Jaccodine (1962). Frank's method is based on the reluctance plot, i.e., an experimentally established polar plot of reciprocal radial shift velocities. Such a plot assumes that a unique radial shift velocity can be assigned to each crystallographic plane. The present interpretation of the residual etch figures in $\{11\bar{2}0\}$ supposes, however, that the radial shift velocity of an F plane at an angle to the surface can have a different value, depending on whether it requires nucleation. If this is correct, the usefulness of a v_r-v_t model, in its present form, might not quite extend to calculations of track geometry. The v_r-v_t model, in contrast to the v_b-v_t model, implies that only the radial shift velocities of the slowest etching planes can be deduced from the geometry and dimensions of etched fission tracks. Attempts to infer the complete polar diagram of etching velocities from track geometry (Yamada et al. 1993) are meaningful only within the context of a v_b-v_t model and should be interpreted with caution.

According to an atomistic model of track revelation in minerals, etching proceeds by a succession of unit steps, each consisting of the removal of an elementary building unit from the crystal surface. This approach offers a basis for the distinction between the different types of surfaces and for the order of their radial shift velocities. Their respective etching properties and several details concerning track geometry, such as the development and evolution of etch pyramids at the track openings (P-type surfaces) and the influence of track orientation on the geometry of the track channels, can be explained to a considerable extent. An atomistic representation of track revelation also involves a limited number of etching velocities: v_{ns}, v_{nd}, v_{ls}, v_{lc}, and v_t. These velocities relate to different processes, and it is hazardous to infer the magnitude of one velocity from measurements of another. In particular, measurements of v_{ls} probably do not provide a reliable estimate of the etching velocity perpendicular to the surface (Singh et al. 1986) or at the track extremity (Laslett et al. 1984).

There is also no obvious relationship between the track-etching efficiency, η, and any of these velocities. The available formulas for calculating η (e.g., Fleischer et al. 1975) are based on a v_b-v_t model and are therefore probably invalid. Even with qualitative assessments of η, inferred from the etching characteristics of the surface (Gleadow 1978, 1981) our limited understanding of track revelation in minerals should be considered. Furthermore, it might be necessary to redefine η because with the identification of residual etch figures, it has become unclear what exactly constitutes an etched fission track. Moreover, even if it were possible to calculate η, this would not constitute a reliable estimate of the track-counting efficiency because the ratio of the track density determined under the microscope to the actual density of tracks intersecting the surface also depends on the track-determination criteria. These, in turn, are partly influenced by the etching conditions and partly by subjective factors. Therefore, we propose to represent the track-counting efficiency by ηq, where η represents etching efficiency and q represents observer efficiency. The two are not separable, and neither η nor q, nor therefore ηq, can be determined from basic assumptions regarding track revelation and observation.

Acknowledgments

The experiments reported in this paper are part of the Ph.D. research of R.J., who is indebted to the Belgian Institute for Science and Technology for its financial support. P.V. is grateful for the support of the Belgian National Fund for Scientific Research. We are pleased to acknowledge R. Maréchal for providing us with crystals of Durango apatite from his private collection. We are also indebted to G. Stoops, L. Fiermans, and A. Vinckier for the use of their electron microscopes, and to D. De Decker, F. Maertens, and W. Bohyn for technical assistance. We thank M. Wagner for providing us with a technique for making high-quality plastic replicas.

References cited

Amelinckx, S. (1955) Microscopic and interferrometric study of crystal surfaces in relation to the theory of dislocations. Ph.D. thesis, State University of Gent, Belgium (in Dutch).

———(1964) The direct observation of dislocations. Solid State Physics, Supplement 6, 3–53.

Batterman, B.W. (1957) Hillocks, pits and etch rate in germanium crystals. Journal of Applied Physics, 28, 1236–1241.

Belyaev, A.D., Bikbova, Z.S., Gayshan, V.L., Khabibullaev, P.K., Kogan, V.I., Pikul, V.P., and Usmandiarov, A.M. (1988) The ion track etching rate in crystal track detectors. Nuclear Tracks and Radiation Measurements, 14, 369–372.

Bennema, P. (1993) Growth and morphology of crystals: Integration of theories of roughening and Hartman-Perdok theory. In D.T.J. Hurle, Ed., Handbook of crystal growth, p. 477–581. Elsevier Science, Amsterdam.

Buck, T.M. (1959) Damaged surface layers: Semiconductors. In H.C. Gatos, Ed., The surface chemistry of metals and semiconductors, p. 107–135. Wiley, New York.

Crowley, K.D., Cameron, M., and Schaeffer, L. (1991) Experimental studies on annealing of etched fission tracks in fluorapatite. Geochimica et Cosmochimica Acta, 55, 1449–1465.

Faust, J.W. (1959) Etching of metals and semiconductors. In H.C. Gatos, Ed., The surface chemistry of metals and semiconductors, p. 151–173. Wiley, New York.

Fleischer, R.L., and Price, P.B. (1964) Techniques for geological dating of minerals by chemical etching of fission fragment tracks. Geochimica et Cosmochimica Acta, 28, 1705–1714.

Fleischer, R.L., Price, P.B., and Walker, R.M. (1975) Nuclear tracks in solids: Principles and applications (1st edition), 604 p. University of California Press, Berkeley.

Frank, F.C. (1958) On the kinematic theory of crystal growth and dissolution processes. In T.H. Doremus, B.W. Roberts, and D. Turnbull, Eds., Growth and perfection of crystals, p. 411–419. Wiley, London, U.K.

Frank, F.C., and Ives, M.B. (1960) Orientation-dependent dissolution of germanium. Journal of Applied Physics, 31(11), 1996–1999.

Franke, W., Heimann, R., and Lacmann, R. (1975) The dissolution forms of single crystal spheres: III. Dissolution of Ge and Si. Journal of Crystal Growth, 28, 151–156.

Gilman, J.J. (1959) Effect of imperfections on dissolution. In H.C. Gatos, Ed., The surface chemistry of metals and semiconductors, p. 137–150. Wiley, New York.

———(1960) Terraces on etch pits. Journal of Applied Physics, 31, 936.

Gleadow, A.J.W. (1978) Anisotropic and variable track etching characteristics in natural sphenes. Nuclear Track Detection, 2, 105–117.

———(1981) Fission track dating methods: What are the real alternatives? Nuclear Tracks, 5, 3–14.

Green, P.F., Bull, R.K., and Durrani, S.A. (1978) Particle identification from track etch-rates in minerals. Nuclear Instruments and Methods, 157, 185–193.

Green, P.F., Duddy, I.R., Gleadow, A.J.W., Tingate, P.R., and Laslett, G.M.

(1985) Fission track annealing in apatite: Track length measurements and the form of the Arrhenius plot. Nuclear Tracks, 10, 323–328.

———(1986) Thermal annealing of fission tracks in apatite: 1. A qualitative description. Chemical Geology, Isotope Geoscience Section, 59, 237–253.

Hartman, P. (1973) On the morphology of crystals. Bulletin de Minéralogie, 161, 195–201 (in French).

———(1978) Structure and morphology. In P. Hartman, Ed., Crystal growth: An introduction. North-Holland Series in Crystal Growth, 1, 367–402.

Heimann, R., Franke, W., and Lacmann, R. (1975) The dissolution forms of single crystal spheres: IV. Dissolution of MgO. Journal of Crystal Growth, 28, 151–156.

Honess, A.P. (1927) The nature, origin and interpretation of the etch figures on crystals, 171 p. Wiley, New York.

Hurford, A.J. (1990) Standardization of fission track dating calibration: Recommendation by the fission track working group of the I.U.G.S. subcommission on geochronology. Chemical Geology, Isotope Geoscience Section, 80, 171–178.

Irving, B.A. (1962) Chemical etching of semiconductors. In P.J. Holmes, Ed., The electrochemistry of semiconductors, p. 256–289. Academic, London, U.K.

Jaccodine, R.J. (1962) Use of a modified free energy theorem to predict equilibrium growing and etch shapes. Journal of Applied Physics, 33(8), 2643–2647.

Jafri, E.H., Qureshi, A.A., Sial, M.A., and Khan, H.A. (1990) Track shapes, etching characteristics and track density distribution on different planes of apatite. Radiation Effects and Defects in Solids, 115, 227–232.

Lacmann, R., Heimann, R., and Franke, W. (1974) The dissolution forms of single crystal spheres: II. Theory for the molecular-kinetics interpretation. Journal of Crystal Growth, 26, 117–121.

Laslett, G.M., Gleadow, A.J.W., and Duddy, I.R. (1984) The relationship between fission track length and track density in apatite. Nuclear Tracks, 9, 29–38.

Laslett, G.M., Green, P.F., Duddy, I.R., and Gleadow, A.J.W. (1987) Thermal annealing of fission tracks in apatite: 2. A quantitative analysis. Chemical Geology, Isotope Geoscience Section, 65, 1–13.

Lovell, L.C. (1958) Dislocation etch pits in apatite. Acta Metallurgica, 6, 775–778.

Maurette, M. (1966) A study of heavy ion tracks in natural minerals of terrestrial and extraterrestrial origin. Bulletin de la Société Française de Minéralogie et Cristallographie, 89, 41–75 (in French).

Maurette, M., Pellas, P., and Walker, R.M. (1964) A study of fossil fission tracks in mica. Bulletin de la Société Française de Minéralogie et Cristallographie, 87, 6–17 (in French).

Paul, T.A. (1993) Transmission electron microscopy investigation of unetched fission tracks in fluorapatite: Physical process of annealing. Nuclear Tracks and Radiation Measurements, 21, 507–511.

Paul, T.A., and Fitzgerald, P.G. (1992) Transmission electron microscopic investigation of unetched fission tracks in fluorapatite. American Mineralogist, 77, 336–344.

Paulick, J., and Newesely, H. (1968) Investigation of the apatite from Cerro de Mercado, Durango, Mexico. Neues Jahrbuch für Mineralogie Monathefte, 7, 224–235 (in German).

Perron, C., and Bourot-Denise, M. (1986) Heavy ion track etch rate measurements and track structure in a mineral. Nuclear Tracks, 12, 29–32.

Price, P.B., and Walker, R.M. (1962) Chemical etching of charged particle tracks. Journal of Applied Physics, 33, 3407–3412.

Sangwal, K. (1987) Etching of crystals: Theory, experiment, and application. In S. Amelinckx and J. Nihoul, Eds., Defects in Solids, 15, 497 p. North-Holland, Amsterdam.

Singh, S., Singh, D., Sandhu, A.S., and Virk, H.S. (1986) A study of etched track anisotropy in apatite. Mineralogical Journal, 13, 75–85.

Somogyi, G. (1980) Development of etched nuclear tracks. Nuclear Instruments and Methods, 173, 21–42.

Terpstra, R.A., Bennema, P., Hartman, P., Woensdrecht, C.F., Perdok, W.G., and Senechal, M.L. (1986) F faces of apatite and its morphology: Theory and application. Journal of Crystal Growth, 78, 468–478.

Thiel, K., and Külzer, H. (1977) Anistropy of track registration in natural feldspar crystals. Radiation Effects, 35, 50–56.

Wagner, G.A. (1969) Tracks from spontaneous fission of ^{238}U as a means for dating of apatites, and a contribution to the geochronology of the Odenwald. Neues Jahrbuch für Mineralogie Abhandlungen, 110, 252–286 (in German).

Wagner, G.A., and Van den haute, P. (1992) Fission-track dating. Solid earth sciences library, 6, 285 p. Kluwer Academic, Dordrecht, the Netherlands.

Yamada, R., Tagami, T., and Nishimura, S. (1993) Assessment of overetching factor for fission track length measurement in zircon. Chemical Geology, Isotope Geoscience Section, 104, 251–259.

Young, E.J., Myers, A.T., Munson, E.L., and Cowklin, N.M. (1969) Mineralogy and geochemistry of fluoroapatite from Cerro de Mercado, Durango, Mexico. U.S. Geological Survey Professional Paper, 650D, 84–93.

Manuscript received November 28, 1995
Manuscript accepted July 30, 1996